A Digital Heterodyne 2- To 150-kHz Measurement Method Based on Multiresolution Analysis

Paul S. Wright and Deborah Ritzmann

***Abstract*— A description is given of a new 2- to 150-kHz range frequency decomposition method, as required to support power grid compatibility level measurements. This real-time digital method is based on a tree structure of nominally identical modular algorithmic elements to provide a decomposition of the signal bandwidth resulting in a 200-Hz resolution. Each modular element divides the bandwidth of its input into a low-frequency and a high-frequency half. Elements connected in the tree result in a progressive increase in resolution at each level of the tree, hence multiresolution analysis. The modular element is based on heterodyning and down-sampling. Simplifications of the modular elements that result in an efficient process of changing the sign of alternate input samples, digital filtering, and discarding alternate samples at the output are presented. It is shown that these cloned modular elements form a computationally efficient algorithm that can operate in real-time. Refinements to cover gaps in the bandwidth which cause errors are explained. The algorithm is compatible with the traditional CISPR 16 analog heterodyne method. Test results are presented which show that the method achieves accuracies of ±5% of reading, as required for compatibility level measurements.**

***Index Terms*— Digital filters, digital signal processing, electromagnetic compatibility (EMC) and interference, power system measurements, power quality (PQ), wavelets.**

I. Introduction

A. Motivation

THE electromagnetic compatibility (EMC) directive [1] and associated regulations aim to prevent interference between electrical appliances causing malfunction or shortening of the service life of other equipment and appliances. In electricity grids, the conducted interference is of concern to utilities that must provide adequate power quality (PQ) for their customers, whilst ensuring grid infrastructure is protected. PQ up to 2 kHz has been regulated for the last two decades by a series of IEC standards including IEC 61000-4-7 [2] for the measurement of harmonics to 2 kHz. In recent years, the increase in the use of power converters for renewable generation, storage systems, and electric vehicles, as well as high-efficiency switch mode power supplies in energy-efficient appliances, has led to an increase in EMC problems in the frequency range 2–150 kHz [3]. This interference can consist of individual frequency tones or broadband emissions. The emissions can be of stable amplitude or can have periodic variations [4]. Laboratory measurements of emissions from individual appliances in the 2- to 150-kHz band can be made using the CISPR 16 radio standard [5] based on the use of an analog superheterodyne [6] receiver which is used to sweep the frequency range. Digital versions of this receiver based on discrete Fourier transforms (DFTs) have also been proposed and implemented [7].

As part of EMC, utilities need to measure the prevailing levels of conducted interference in electricity grids in order to assess compatibility levels [8], make planning decisions, and to settle customer complaints. Various working groups of EMC standards committee IEC SC77A have expressed the requirement that these grid PQ measurements should be compatible with CISPR 16 and there is a current initiative to develop a normative annex to the PQ measurements standard IEC 61000-4-30 [9] to specify a 2- to a 150-kHz method for implementation in PQ analyzers.

This article describes a proposed method based on a digital superheterodyne which is directly compatible with CISPR 16.

B. Existing 2- To 150-kHz Measurement Methods

The CISPR 16 method can be digitally implemented, an overview of a DFT-based method is given in [7] and such digital receivers have been implemented by several commercial vendors for laboratory use. CISPR 16 specifies the accuracy of ±2 dB which is equivalent to +26% and −21% of reading, whilst IEC 61000-4-7 [2] specifies the accuracy of ±5% of reading, so there is a significant difference between the radio regulatory use and the expectations of PQ engineers who need to plan and manage customer loads for utilities.

Processing speed and memory storage requirements are also noteworthy considerations for a suitable method, especially if it is to be retrofitted to existing PQ instrumentation or data acquisition platforms. For compatibility level measurements, prolonged measurement surveys are required by utilities [8] and a suitable method must be capable of real-time processing with no gaps and interruptions as specified in IEC 61000-4-7 [2]. However, the 150-kHz bandwidth implies sampled data rates of at least 300-kilo samples per second (kS/s) which is highly challenging in terms of real-time data handling, processing, and visualization. These requirements are a challenge to the practicality of published methods,

Manuscript received August 18, 2020; revised October 23, 2020; accepted November 5, 2020. Date of publication November 16, 2020; date of current version January 6, 2021. This project (18NRM05 SupraEMI) has received funding from the EMPIR programme co-financed by the Participating States and from the European Union's Horizon 2020 research and innovation programme. The Associate Editor coordinating the review process was Dr. Dimitrios Georgakopoulos. *(Corresponding author: Paul S. Wright.)*

The authors are with the National Physical Laboratory, Teddington TW11 0LW, U.K. (e-mail: paul.wright@NPL.co.uk).

Digital Object Identifier 10.1109/TIM.2020.3038290

including a technique based on wavelets [10] and algorithms based on compressive sensing techniques [11], which could be considered as suitable methods, although they are not compatible with CISPR 16. Short-time FT methods [13] have the potential for real-time implementation but do not give time-domain outputs.

A direct digital implementation of the CISPR 16 heterodyne using digital mixers and digital filters has been proposed by Bergeron [12]. This is highly attractive because of its direct compatibility with its analog predecessor. However, if measurements with the CISPR 16 frequency resolution of 200 Hz over the full 2-to 150-kHz band are required, this implies 741 of each: mixers, sine, and cosine lookup tables and digital filters all processed at data rates of >300 kS/s. Unless the digital filters are very high order, there will be significant gaps between the 200-Hz bands where signals will be highly attenuated resulting in gross negative errors. A solution involving overlapping windows in the frequency domain to cover the gaps implies a doubling of these processing requirements.

C. Outline of Article

This article is an extension of a proceedings article [14] and building on the concept presented there, this article proposes a direct digital implementation of the CISPR 16 method but optimized for processing efficiency using the principles of multiresolution analysis (MRA) [15] as used in [10]. The algorithm that is described is relatively simple in nature and intuitively easy to understand. This simplicity is highly attractive from the point of view of the need to specify in international standardization and for ease of implementation.

Section II gives a résumé of the underlying classical techniques which are used in the proposed measurement method including heterodyning, MRA, down-sampling, described in Sections II-A–II-C, respectively. Section II-D describes a modular element that makes up the MRA algorithm which is then connected in a tree structure of these largely identical processing elements to form the full analysis algorithm as described in Section II-E with output post processing options described in Section II-F. Adaption of the algorithm to provide overlaps in the frequency domain for the purposes of covering "gaps" between the 200-Hz resolution bands is described in Section II-G.

Section III gives specific implementation details on how to make a realizable measurement with the algorithm, including information on digital filters and parallel computing architecture that can be used on multicore microprocessor systems.

Section IV describes algorithm testing using repetitive and nonrepetitive waveforms. Processing speed performance is also discussed.

II. Description of the Measurement Method

The proposed digital method is based on three signal processing methods, namely heterodyning, multiresolution analysis, and down-sampling. In the proposed method these are brought together to develop a modular element whose outputs divide the input signal bandwidth into a high and low half. A number of these modular elements are connected in a tree structure to give a dyadic decomposition of the frequency bandwidth.

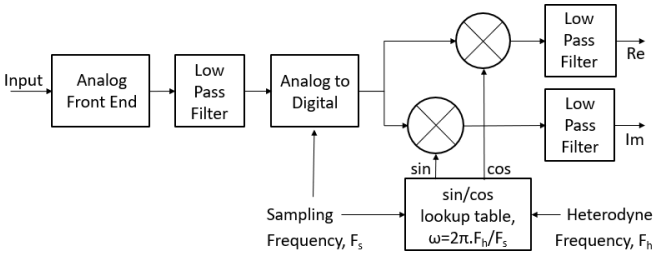

Fig. 1. Quadrature multiplying digital heterodyne giving discrete bandlimited, frequency shifted Re and Im part outputs.

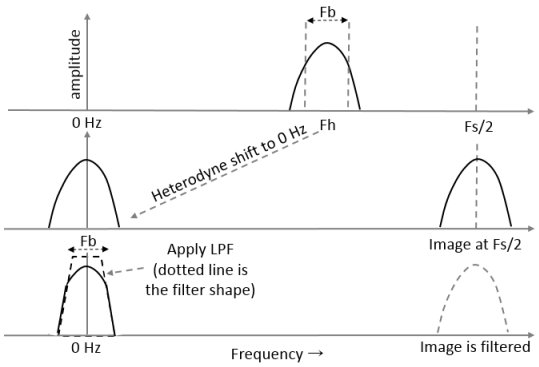

Fig. 2. Heterodyne spectrum with a band shift to 0 Hz and filtering.

A. Heterodyning

Heterodyning [6] as used in analog or digital radio receivers, takes a frequency band centered on a given frequency and shifts it to a new center frequency using a multiplying mixer with an oscillator frequency (F_h) as shown in Fig. 1.

As described in Section I, analog heterodyne schemes are the basis of the CISPR 16 method. Digital heterodyne schemes are widely used in signal processing to shift bands of frequency to the baseband (centered around 0 Hz) and are often implemented using quadrature multiplication (sometimes known as I/Q demodulation or weaver demodulation). Quadrature multiplication was used as the basis of interharmonic analysis in [16] and [17] and is the basis of the phasor measurement unit [18].

In Fig. 1, the multiplication is performed using a quadrature multiplying pair using the real (Re) (cos) and imaginary (Im) (sin) parts of the mixing frequency to form "sum" and "difference" tones as given in the following equation for the "Re" part of a signal x:

$$\begin{aligned}\mathrm{Re}(x) &= \sin\left(2\pi F_b'\right)\cdot\cos(2\pi F_h)\\ &= 0.5\left[\sin\left(2\pi F_b' + 2\pi F_h\right) + \sin\left(2\pi F_b' - 2\pi F_h\right)\right] \quad (1)\end{aligned}$$

where F_b' is any frequency in the F_b band shown in Fig. 2. A corresponding sum and difference equation follows the "Im" part.

As seen in Fig. 2 [14], to select a bandwidth F_b centered on F_h, the oscillator frequency is set to F_h, and the resulting difference frequency (1) will be centered on 0 Hz, a low-pass filter (LPF) can then be used to select the required

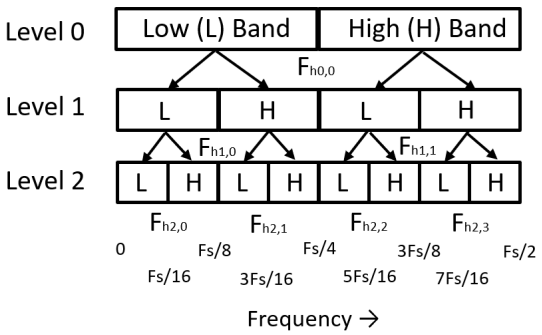

Fig. 3. MRA tree progressively dividing the frequency band at each level. $F_{\mathrm{hl},b}$ are the heterodyne frequencies used at each level and band. The x-axis frequencies are also shown in terms of the sampling frequency F_s.

bandwidth F_b. For example, to measure all the frequency components between 2 and 2.2 kHz, F_h would be set to 2.1 kHz and the bandwidth of the LPF would be set to 100 Hz. The resulting heterodyned band centered around 0 Hz between -100 and $+100$ Hz would remain and all other frequencies, including the sum (1), will be attenuated by the LPF. F_s in Fig. 1 is the sampling frequency of the analog-to-digital converter (ADC) and spectral "images" produced by the heterodyne process are also attenuated by the LPF.

The quadrature multiplying pair is required because the desired frequency translation is centered around 0 Hz and overlapping real and quadrature bands allow for a noninverted spectrum at negative frequencies.

In the context of this application, multiple heterodynes could be used with different F_h mixer frequencies, to shift each frequency band of interest in the 2- to 150-kHz band, down to 0 Hz. As described in Section I, to use heterodynes to divide 2 to 150 kHz into 200-Hz widebands, would require 741 heterodynes with associated LPFs.

The accuracy of the method is determined by the LPF response which should include a cutoff which should be as sharp as possible, with the filter passband gain as flat as possible, implying a high-order LPF. This implies 741 heterodynes, each containing two high-order LPFs, exposed to a sample rate of at least two times 150 kHz, which makes real-time processing is highly challenging.

B. Multiresolution Analysis

MRA [15] was devised for use with wavelets and is effectively a hierarchy of bandpass filters that break the measurement spectrum into a tree structure, progressively dividing the bandwidth at each level of the tree into a low and high half. The MRA divided spectrum is shown in Fig. 3 [14].

MRA analysis using wavelets has been applied to 2- to 150-kHz measurements in [10], in a similar way heterodynes can use a classical LPF at each level to perform the MRA.

C. Down-Sampling

The LPF processing speed can be improved by reducing the sample rate, but this is not allowed under the Nyquist restrictions. However, after the LPF in the heterodyne, the signal bandwidth is reduced and down-sampling can be used to

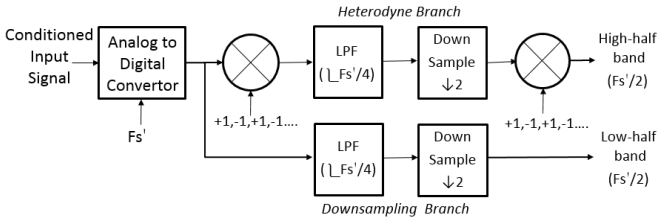

Fig. 4. One modular element of the MRA method. Input is a sampled waveform at sample rate F_s'; output is high and low band-limited sampled waveforms at $F_s'/2$.

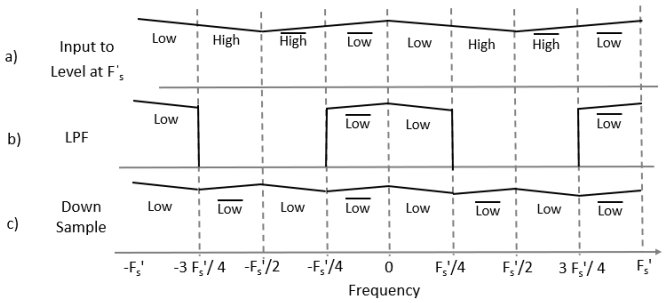

Fig. 5. MRA down-sampling branch frequency spectrum, a classical down-sampling by two operation. The y-axes are amplitude. (b) and (c) show how the frequency spectrum shown in (a) is modified at the outputs of the various blocks in the lower-half, downsampling branch of Fig. 4.

reduce the computational burden of subsequent MRA levels (there are less samples to process) and also allows the LPF specification to be relaxed at lower levels. This classical multirate signal processing approach [19] can give a significant processing speed advantage in this application.

D. Implementation of an MRA Element

Based on Sections II-A–II-C, a basic MRA modular element was devised that takes input samples (at F_s' sampling rate) and splits the bandwidth into low and high halves, outputting two sample sequences at half the sampling rate (F_s'/2) of the input. This modular element is, in principle, cloned throughout the MRA tree.

Fig. 4 shows how each element of the low and high pass operation can be implemented. The signal path splits into two branches after the ADC. A heterodyne branch is a simplified form of the heterodyne in Fig. 1 which functions to select the high half of the frequency band. The down-sampling-branch is a classical down-sampler [19] which functions to select the low-half of the frequency band as shown in Fig. 5.

Fig. 5(a) shows the frequency band of the sampled input signal. The spectrum between 0 and F_s'/2 is shown with a downward sloping amplitude for illustrative purposes to highlight the mirroring that occurs around zero and at the F_s'/2 Nyquist frequency. These mirrored spectra are inverted shown by the upward slope. The objective of the down-sampling-branch of the MRA element is to select the lower half of the frequency spectrum between 0 and F_s'/4 indicated by the word "Low" in Fig. 5, whilst removing the upper half indicated by the word "High."

Fig. 5(b) shows a perfect LPF operation which removes the high half and its mirror images. The down-sample by two operations, where every second sample is discarded, results in

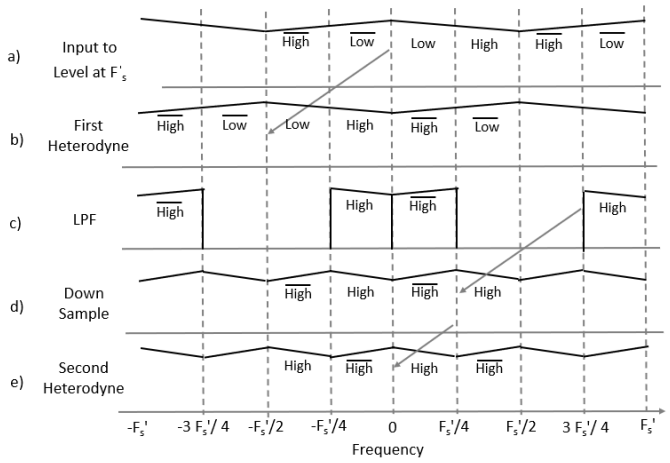

Fig. 6. MRA upper-half branch frequency spectrum. The y-axes are amplitude. (b)–(e) show how the frequency spectrum shown in (a) is modified at the outputs of the various blocks in the upper-half, heterodyne branch of Fig. 4.

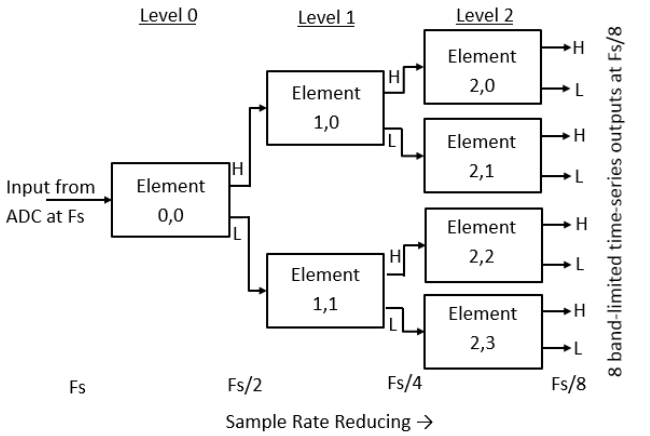

Fig. 7. Tree structure of connected Fig. 4 modular MRA elements to form a three-level MRA scheme.

the spectrum shown in Fig. 5(c) where the mirroring occurs at zero and the new Nyquist frequency of F_s'/4. The output of the lower half MRA element is therefore the lower half frequency band at half the input sampling frequency.

The operation of the heterodyne-branch of the MRA element shown in Fig. 4 can be understood by referring to the frequency spectrum in Fig. 6. Fig. 6(a) is the sampled input signal band and is the same as Fig. 5(a). In this implementation of the digital heterodyne, it is efficient not to shift the upper frequency to be centered around 0 Hz as in Fig. 2, but instead shift it to occupy the lower half-band as shown in Fig. 6(b). This avoids the need for one of the two quadrature branches in Fig. 1 at the expense of losing the phase information which is not required in this application.

Fig. 6(b) shows the result of the first heterodyne which shifts the frequency bands by the heterodyne mixing frequency (F_h) which is set to F_s'/2. This simplifies the $\omega = 2\pi \cdot F_h/F_s$ in Fig. 1 cosine lookup table to $\omega = \pi$, such that $\cos(\omega.n)$ simplifies to a repeating sequence of ± 1s or -1^n, where n is the sample number. So, the first heterodyne operation can be reduced to the high computational efficient operation of changing the sign of every second sample.

Fig. 6(c) shows a perfect LPF operation which removes the low half and its mirror images [see Fig. 5(b)]. The downsample by two operations, where every second sample is discarded, results in the spectrum shown in Fig. 6(d) [see Fig. 5(c)]. Mirroring occurs at zero and the new Nyquist frequency of F_s'/4, but unfortunately leaves the spectrum inverted such that the "bar High," rather than the "High," is in the section between 0 and F_s'/4. In practice, this means that an input signal with a frequency near the bottom of the upper-half band would appear at the output at a frequency near the top of the upper-half band.

Therefore, the frequency spectrum needs to be shifted using a second heterodyne operation by F_s'/4 resulting in Fig. 6(e). As the Nyquist frequency was reduced by two, by downsampling, the mixing frequency for the second heterodyne is once again a repeating sequence of ± 1 multiplications.

The output of the upper-half MRA element is therefore the upper-half frequency band at half the input sampling frequency. The algorithm for the MRA element essentially consists of two identical LPFs, two sign-change operations, and two sample-discarding operations. The computational complexity is therefore almost entirely due to the LPF operations and the designer has a tradeoff choice of algorithm speed against accuracy which is set by the filter order and filter window choice.

E. Heterodyne-Based MRA Measurement Method

In principle, these MRA elements are identical for the whole processing tree, including the filter breakpoints.

The MRA elements are connected in a tree structure as shown in Fig. 7 [14]. In this illustrative example with three levels, the spectrum is split into eight bands at the output of level 2. Note that the sampling rate is halved after each level, the number of elements doubles at each level, and the amount of data that needs to be processed by each MRA element halves.

The MRA methods give rise to the division of the frequency spectrum as shown in Fig. 3. At level 0 in Fig. 3, the high and the low band output response can be seen with the transition at halfway at F_s/4 where the upper band is limited to F_s/2 as seen on the x-axis. The output at level 2, gives the signal split into eight-bands for post processing and display.

The outputs of each level are time-domain functions. As an illustrative example, consider a sinewave input signal with a frequency halfway between F_s/4 and 5 F_s/16. The resulting level 2 output would be a signal in the fifth-band of level 2, appearing as a sinewave output with a frequency of F_s/32 (half the width of the level 2 bands). By contrast, an input signal with a frequency *quarter* of the way between F_s/4 and 5F_s/16 would again in the fifth-band of level 2, but at a frequency of *quarter* of the width of the level 2 bands at F_s/64.

F. Output Postprocessing

The outputs of each level are smoothly varying time-domain functions which are convenient for the measurement of fluctuations of the input signal components. Amplitude fluctuations slow enough to be represented within the available bandwidth of the output level (the bandwidth of level 2 in this example), can be observed at the output time-domain signal.

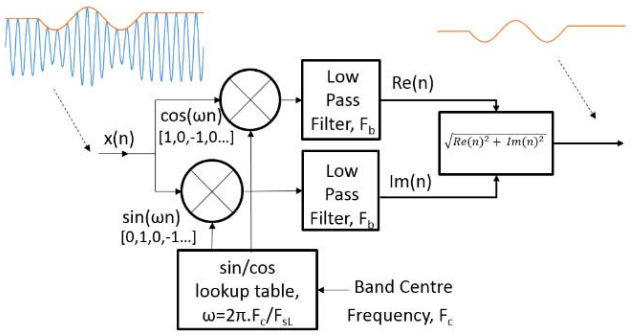

Fig. 8. Heterodyne envelope detector. F_c is the center frequency of the given output band. F_b is the bandwidth of the filters and F_{sL} is the sampling frequency at the output level. For $F_c/F_{sL} = 4$, the sin/cos lookup table can be replaced with the bracketed sequence of 1s and 0s.

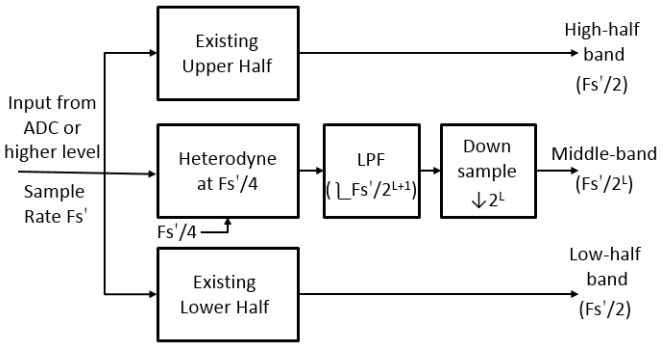

Fig. 9. Modular element of the MRA method with overlapping middle band.

Postprocessing of the eight level-2 bands could simply be the calculation of the rms value of each band-limited signal in each band. In this example, this would give eight rms values for the frequency spectrum comparable to a modulus Fourier transform. Fluctuating signals could be measured by periodically taking contiguous rms values of the continuous signals in each band to give a time series for each of the eight bands in the lowest level, this is comparable to a spectrogram.

However, the calculation of the rms value of the real-valued time-domain signal in each band relies on the knowledge of the signal period, which is unknown. This problem can be solved in the same way as the original CISPR 16 analog heterodyne instrument by making use of an envelope detector. Envelope detectors effectively extract the modulation signal from the modulated carrier (Fig. 8). The signal envelope can be readily obtained by taking the modulus of the Re and Im parts of the signal if they exist.

This complex sample pair is available from the quadrature heterodyne shown in Fig. 1, however, the quadrature part was discarded to improve computational efficiency as is required for the high sample rates present at the highest levels of the method. As the rms value is only required for output at the lowest level of the instrument, where the sampling rate is at its lowest, the missing Im part can be replaced by using a further heterodyne [20] as shown in Fig. 8.

Because of the low sampling rate F_{sL} at the lowest level of the instrument, the envelope detector has much reduced computational overhead compared to the alternative of implementing full quadrature heterodynes (as Fig. 1) throughout the multiple levels. For each output band in turn, Fig. 8 envelope detector heterodyne mixing frequency F_c is set to the center of the given 200-Hz band. The bandwidth of the filters in Fig. 8 (F_b) should be set to reject frequencies above F_c. For example, if the lowest level bandwidth is 200 Hz, F_c is set to 100 Hz, and the filter −3-dB bandwidth to 100 Hz. In this example, the lowest level sampling frequency F_{sL} is 400 Hz, and the sin and cos heterodyne lookup table value of angular frequency is therefore $\omega = \pi/2$, so that the look-up tables can be replaced with a multiplying sequence of 0's, 1's, and −1's as shown in Fig. 8.

Instead of or in addition to these integral outputs, the peak and quasi-peak (QP) values of each band can be calculated. QP outputs are defined in CISPR 16 [5] and can be implemented digitally using a pair of cascaded first-order LPFs as in [21].

G. Overlapping Frequency Bands

In practice, the LPFs do not have perfectly sharp cutoff characteristics and this will cause gaps at the band transitions of the divided spectrum (Fig. 3). Any frequency component that falls in these gaps will be measured with an error.

To cover the gaps, overlapping frequency bands for each transition can be added as an extra horizontal branch as shown in Fig. 9 (see Fig. 4), centered between the other two bands by using a heterodyne frequency of F_s'/4.

This overlapping band would then need to be down-sampled at each level, requiring a subsequent "decimation" LPF at each level to avoid aliasing. It is more efficient to adjust the breakpoint of this LPF to take into account all the subsequent down-sampling of each of the levels below, thus avoiding multiple filtering. As down-sampling by two requires an LPF with a breakpoint of F_s'/4, halving at each of the $L - 1$ levels below the current level, the breakpoint of an LPF to perform the required band-limiting is $F_s'/2^{L+1}$ for an MRA system with L levels.

The F_s/4 heterodyne shown in Fig. 9 will shift the overlapping middle band to be centered around 0 Hz as shown in Fig. 2. This requires the full quadrature heterodyne implementation as shown in Fig. 1 to be used, where F_h in this case is F_s/4. The alternative nonzero-centered approach used in Fig. 4 would not benefit from the simple repeating 0's, 1's, and −1's multipliers, but instead would require a many-valued cosine lookup table to be used. In cases where memory storage is not limiting, this may be a preferable option as it uses one less LPF per element (as it does not require both cos and sin branches).

As can be seen in Fig. 10, the low and high outputs are at the half-stage sampling frequency and are fed to the next level in the MRA tree; whereas the middle output is fed directly to the lowest level and is down-sampled to the output frequency of the lowest level.

III. Implementation for a 2- To 150-kHz PQ Instrument

The illustrative example shown above has just three levels providing 15 output bands as shown in Fig. 10. As the

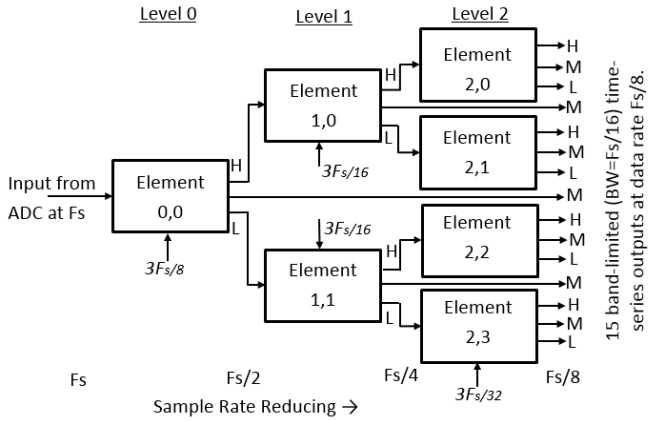

Fig. 10. Illustrative three-level MRA with overlapping output bands using the connected modular elements shown in Fig. 9.

system is modular, this is readily scaled-up to give the required resolution for a PQ instrument. For a system that gives 200-Hz frequency resolution across the 2- to the 150-kHz band, ten levels are required with an input sampling frequency of 409.6 kHz. This gives rise to 1439 output bands (740 high/low bands and 739 middle bands) over a frequency range of 0 Hz to 204.8 kHz, the bands outside of 2–150 kHz are not required and where possible, the tree structure can be simplified to improve calculation speed. The sample rate reduces at each level by a factor of two such that the tenth level is reduced to 200 S/s.

A. Digital Filters

Infinite impulse response LPFs are used in this implementation using the classical biquad architecture [22]. Higher-order filters are required for the topmost level of the algorithm as relatively poor roll-off will propagate through the levels and lead to relatively wide gaps at the lower levels. The filter orders can be progressively relaxed through lower levels.

Many different filter windows are available and in this implementation, a Type-II Chebyshev window [23] has been selected for its ripple-free passband response.

Selecting the filter order is a tradeoff of accuracy versus processing speed. In this application, accuracy of $\pm 5\%$ of reading was set as a target value as it is used for existing PQ instruments below 2 kHz. The order used at each level was selected to achieve the target accuracy when used in conjunction with the middle-band filters (Fig. 9) which were chosen to be fourth order. This tuning process involves an iteration of the filter order and the middle-band filter breakpoint and must be carried out at each level. This resulted in top-level filters of 76th order which are progressively relaxed through the ten levels finishing at fourth order for the bottom level (the same order as the middle-band filters). This is a significant computational burden when it is considered that these top-level filters are exposed to an input sample rate of 409.6 kS/s.

B. Parallel Computing Architecture

Most microprocessors have multiple cores which can be exploited for parallel processing operations, commonly implemented using multiple threads. Furthermore, field programmable gate arrays (FPGAs) allow for many levels of parallel processing. The implementation of the algorithm described in this article concentrates on a Windows PC implementation in common with some existing PQ instruments and as a proof of concept.

At the expense of memory storage, the algorithm can be run in multiple threads by making use of a buffer system. This is achieved as follows.

1) An initial set of samples numbering the width of the buffer is sent to a first thread for calculation of the topmost level, storing the result in an output buffer, whilst further incoming real-time samples are stored in a second input buffer.
2) Upon completion of the calculation by the first thread, it is set to work with a new calculation on the second input buffer set of samples, with further incoming samples stored in the first input buffer.
3) Also on completion of the first thread, its output buffer is used as the input buffer to another thread that takes care of the next lower levels performing their calculations and storing the results in further output buffers and so on.
4) The number of threads can be extended to optimize the processing such that each thread takes a similar length of time to compute so that they all finish at a similar time. Threads and buffers can then be recycled once their data are no longer required.
5) A further thread can be used to calculate the output processing (rms and QP) and to display/store results.

The size of the buffers and the number of buffers needs to be adjusted to ensure they do not overflow with the incoming sample stream. As nonreal time operating systems are nondeterministic in timing, optimizing buffer configurations needs careful consideration.

Processors such as those with six cores (12 logical processors) could use one thread for input data handling, one thread for output processing, and the remainder used for the ten levels. This implementation results in a processing time of approximately 0.45 s for 1 s of sampled input data when using a six-core i7 2.6-GHz Windows laptop (better than twice the speed required for real-time).

IV. Testing and Results

To demonstrate the performance of the system a number of test signals were considered.

A. Single Tone Tests

The basic accuracy of the method throughout the frequency range can be assessed by applying single-tone constant amplitude sine wave signals at a range of frequencies. It is particularly important to concentrate on the gaps between the higher level frequency bands (i.e., halfway at level 0, quarters at level 1) where it is the most challenging to tune the digital filters to avoid significant errors. It is also important to check accuracy using test signals with frequencies which are not integer multiples of frequency resolution (i.e., interharmonics).

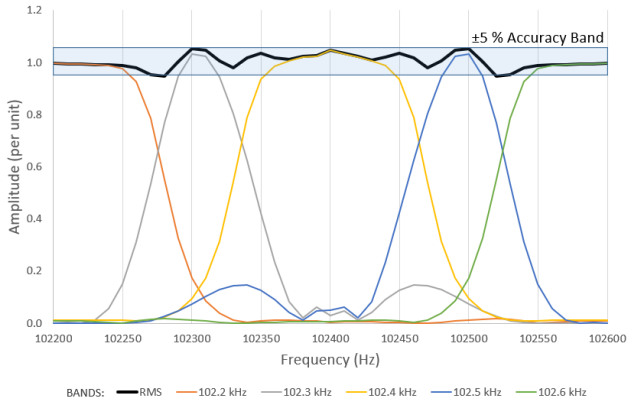

Fig. 11. RMS output for frequency swept across the center of frequency range in 10-Hz steps. A ±5% accuracy band shown. The colored plots are the output of the five bands of the algorithm in the center of the frequency range.

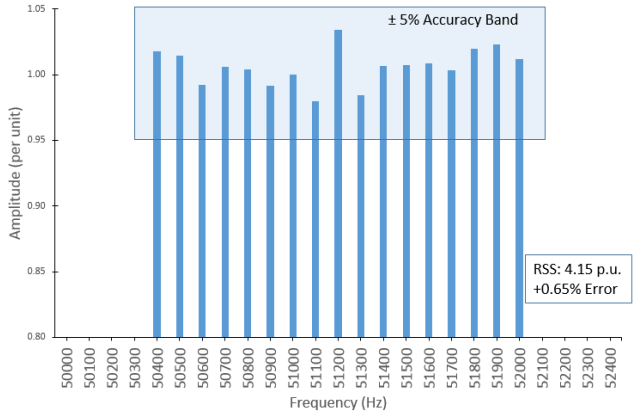

Fig. 12. Analysis of a multitone signal. A ±5% accuracy band shown.

A plot of the center of the 204.8-kHz bandwidth is shown in Fig. 11 where the interaction between the overlapping bands has maintained the rms value in an envelope of about ±5% of reading, demonstrating preservation of input signal energy to this accuracy level. After allowing sufficient time for the digital filters to settle (see Section IV-C), the rms value of the total signal was calculated using the root sum square (RSS) of all the output components. Some stopband overshoot is visible for 102.3- and 102.5-kHz bands; whilst this makes only a small difference (≈0.005 p.u.) to the rms value (≈0.1 added by squares to ≈1), there is some room for improvement to these filters.

B. Multitone Test

In this test, a signal of 17 added sinusoidal signals each of unit amplitude was used. The signal components were spaced in 100-Hz frequency steps, centered on 51.2 kHz, i.e., the quarter point of the 204.8-kHz bandwidth. The phases of the signal components were varied in $\pi/8$ steps, such that the center frequency has zero phase and the lowest and highest components have phases of $-\pi$ and π, respectively. The theoretical rms value of this 17 component waveform is $\sqrt{17}$.

The result of the analysis of this signal is shown in Fig. 12 which shows the ±5% target amplitude accuracy

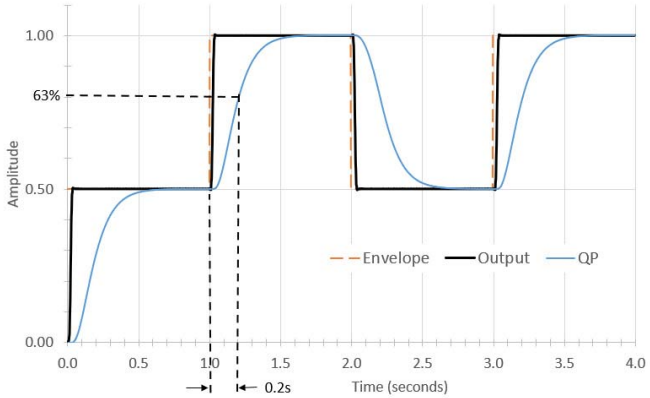

Fig. 13. Response to a fluctuating signal. A single frequency sinewave is modulated by the "Envelope" and the "Output" response of the algorithm relevant frequency bin is shown settling to its final amplitude in approximately 35 ms. The CISPR QP detector output is also shown with a 63% time constant of approximately 0.2 s.

for each individual frequency component. The RSS value was found to be +0.65% in the error of the theoretical rms value.

C. Step Change in Amplitude Test

In this test, the performance of the algorithm to a fluctuating amplitude signal was assessed. A single frequency test signal was used which can be any frequency in the measurement range (14.1 kHz was used in this example). The signal amplitude was modulated by a step-change envelope function as shown in Fig. 13. The output of the algorithm's relevant band is plotted in Fig. 13 where the time taken to follow the step-changes was assessed to be approximately 35 ms. This delay is caused by the rise time of the chosen length of digital filters used in the algorithm and could be optimized if required, although it is considerably faster than the traditional method [2] used for low-frequency harmonics that includes a 1.5-s low pass filter.

The CISPR 16 QP detector can be readily implemented on the output data. Traditionally this is an analog circuit but several implementations using digital filters exist and in this case the implementation given in [21] was used and the resulting output is shown in Fig. 13 with a time constant of approximately 0.2 s as specified in CISPR 16.

V. Conclusion

The method presented in this article is an effective and simple algorithm which can be readily tuned to achieve a desired level of accuracy balanced against computational speed. As required by the EMC community, it is fully compatible with the historical CISPR 16 method that was also based on a heterodyne.

At its simplest, the algorithm consists of a tree of nominally identical modular elements (Fig. 4). Each element splits its input signal bandwidth into a high- and low-frequency half. This is achieved by a process of changing the signs of the samples, applying two digital filters, and then discarding samples.

In practice, each level of the tree will have digital filters of different order and gaps in the output frequency response at the edges need to be filled by an overlapping stage.

The method provides continuous time-domain outputs of each frequency which is ideal for measuring the modulation functions of nonstationary waveforms. These time-domain outputs can be readily processed for peak, QP, rms, and integral values as required by the given application.

The algorithm has been implemented as a Windows application and it runs in real-time on a multicore laptop computer.

The next steps for this work involve embedding the algorithm in a standalone 2- to 150-kHz instrument that can be used for grid compatibility measurements. Some further work using different filter windows and other optimizations could improve accuracy and computational efficiency.

REFERENCES

[1] (Feb. 2014). *Directive 2014/30/EU of the European Parliament and of the Council*. Accessed: Oct. 20, 2020. [Online]. Available: https://eur-lex.europa.eu/eli/dir/2014/30/oj

[2] *Electromagnetic Compatibility (EMC)—Part 4–7: Testing and Measurement Techniques*, IEC Standard 61000-4-7, 2002.

[3] V. Ravindran, T. Busatto, S. K. Roönnberg, J. Meyer, and M. H. J. Bollen, "Time-varying interharmonics in different types of grid-tied PV inverter systems," *IEEE Trans. Power Del.*, vol. 35, no. 2, pp. 483–496, Apr. 2020, doi: 10.1109/TPWRD.2019.2906995.

[4] I. Fernández, D. de la Vega, A. Arrinda, I. Angulo, N. Uribe-Pérez, and A. Llano, "Field trials for the characterization of non-intentional emissions at low-voltage grid in the frequency range assigned to NB-PLC technologies," *Electronics*, vol. 8, no. 9, p. 1044, Sep. 2019.

[5] *Radio Disturbance and Immunity Measuring Apparatus*, Standard CISPR 16-1-1, 2019.

[6] L. C. Godara, "Introduction to 'The heterodyne receiving system, and notes on the recent Arlington-Salem tests,"' *Proc. IEEE*, vol. 87, no. 11, pp. 1975–1978, Nov. 1999.

[7] *Specification for Radio Disturbance and Immunity Measuring Apparatus and Methods—Background on the Definition of the FFT-Based Receiver*, Standard CISPR TR 16 3:2010+A2:2015, pp. 207–227.

[8] *Compatibility Levels for Low-Frequency Conducted Disturbances and Signalling in Public Low-Voltage Power Supply Systems*, IEC Standard 61000-2-2, 2002.

[9] *Testing and Measurement Techniques—Power Quality Measurement Methods*, IEC Standard 61000-4-30, 2015.

[10] S. Lodetti, J. Bruna, J. J. Melero, V. Khokhlov, and J. Meyer, "A robust wavelet-based hybrid method for the simultaneous measurement of harmonic and supraharmonic distortion," *IEEE Trans. Instrum. Meas.*, vol. 69, no. 9, pp. 6704–6712, Sep. 2020, doi: 10.1109/TIM.2020.2981987.

[11] S. Zhuang, W. Zhao, R. Wang, Q. Wang, and S. Huang, "New measurement algorithm for supraharmonics based on multiple measurement vectors model and orthogonal matching pursuit," *IEEE Trans. Instrum. Meas.*, vol. 68, no. 6, pp. 1671–1679, Jun. 2019, doi: 10.1109/TIM.2018.2878613.

[12] R. Bergeron, *Private Communication*, IEC Standard SC77A WG9, Jun. 2020.

[13] M. Schwenke and D. Klingbeil, "Application aspects and measurement methods in the frequency range from 9 kHz to 150 kHz," in *Proc. 25th Conf. Electr. Distrib. (CIRED)*, 2019, pp. 2–6.

[14] P. S. Wright and D. Ritzmann, "A digital heterodyne 2-150 kHz measurement method," in *Proc. Conf. Precis. Electromagn. Meas. (CPEM)*, Boulder, CO, USA, Aug. 2020.

[15] S. G. Mallat, *A Wavelet Tour of Signal Processing*, New York, NY, USA: Academic, 1999.

[16] P. S. Wright, "Interharmonics analysis and measurement methods applied to mains frequency compliance testing," *IEE Proc. Sci., Meas. Technol.*, vol. 153, no. 6, p. 248–255, Nov. 2006.

[17] P. S. Wright, "Testing electrical apparatus," British Patent GB 2 372 821, Nov. 10, 2000.

[18] *IEEE Standard for Synchrophasor Measurements for Power Systems*, IEEE Standard C37.118.1a-2014, 2014.

[19] E. C. Ifeachor and B. W. Jervis, "Sampling rate reduction: Decimation by integer factors," in *Digital Signal Processing: A Practical Approach*, 1st ed. Reading, MA, USA: Addison-Wesley, 1993, p 494.

[20] R. Lyons. *Asynchronous Complex Envelope Detection*. Accessed: Jun. 30, 2020. [Online]. Available: https://www.dsprelated.com/showarticle/938.php

[21] S. Braun, F. Krug, and P. Russer, "A novel automatic digital quasi-peak detector for a time domain measurement system," in *Proc. Int. Symp. Electromagn. Compat.*, vol. 3, Silicon Valley, CA, USA, 2004, pp. 919–924, doi: 10.1109/ISEMC.2004.1349948.

[22] E. C. Ifeachor and B. W. Jervis, "Practical building blocks for IIR filters," in *Digital Signal Processing: A Practical Approach*, 1st ed. Reading, MA, USA: Addison-Wesley, 1993, p. 418.

[23] E. C. Ifeachor and B. W. Jervis, "Chebyshev filter," in *Digital Signal Processing: A Practical Approach*, 1st ed. Reading, MA, USA: Addison-Wesley, 1993, p. 395.

Paul S. Wright received the B.Sc. and Ph.D. degrees in electrical and electronic engineering from the University of Surrey, Surrey, U.K., in 1987 and 2002, respectively.

He spent three years as a Research Fellow with the University of Surrey, where he was involved in the field of spacecraft sensors and attitude control. This was followed by three years with the Central Electricity Research Laboratory, where he was involved in advanced control systems. In 1992, he joined the National Physical Laboratory, Teddington, U.K., where he is currently a Principle Research Scientist specializing in ac measurements and waveform analysis. He has coordinated five EU collaborative Research and Development projects and he is currently a coordinator of the EU project on 2- to 150-kHz grid measurement SupraEMI of which this work is part.

Deborah Ritzmann received the B.Sc. degree in mathematics and physics from the University College London, London, U.K., in 2012, and the Ph.D. degree in synchrophasor-based overhead line impedance measurement for dynamic line rating applications from the University of Reading, Reading, U.K., in 2017, in collaboration with the National Physical Laboratory, Teddington, U.K..

She subsequently worked in the electricity industry for the British transmission system operator National Grid ESO and renewable generation developer Anesco. She joined the National Physical Laboratory in 2019, where she is currently a Higher Research Scientist contributing to research projects in the field of electricity networks metrology.